Complexes of the Ruthenium(II)−2,2′:6′,2″-Terpyridine Family. Effect of Electron-Accepting and -Donating Substituents on the Photophysical and Electrochemical Properties

Mauro Maestri,*[1a] Nicola Armaroli,[1a] Vincenzo Balzani,*[1a] Edwin C. Constable,*[1b] and Alexander M. W. Cargill Thompson[1b]

Dipartimento di Chimica "G. Ciamician", Università di Bologna, I-40126 Bologna, Italy, and Institut für Anorganische Chemie der Universität, Basel, CH-4056, Switzerland

Received December 29, 1994[⊗]

We have investigated the luminescence properties of 14 $[Ru(tpy\text{-}X)(tpy\text{-}Y)]^{2+}$ complexes (tpy = 2,2′:6′,2″-terpyridine; X = Y = $MeSO_2$, Cl, H, Ph, EtO, OH, or Me_2N; X = H, Y = $MeSO_2$; X = OH, Y = $MeSO_2$; X = Cl, Y = EtO; X = OH, Y = Ph; X = $MeSO_2$, Y = Me_2N; X = Cl, Y = Me_2N; X = OH, Y = Me_2N; Me = CH_3; Et = C_2H_5; Ph = C_6H_5). All the complexes examined display a strong luminescence in rigid matrix at 77 K, with lifetimes in the 1−10 μs time scale. The energy of the emission maximum is red shifted for both electron-accepting and electron-donating substituents compared to that of the parent $Ru(tpy)_2^{2+}$ complex. At room temperature, electron-accepting substituents increase the luminescence quantum yield and the excited state lifetime, whereas electron-donating substituents show an opposite effect. The temperature dependence of the emission lifetime has been investigated for some representative complexes, and the role played by activated and activationless nonradiative transitions is examined. It is shown that the values of rate constants for radiationless decay from the luminescent excited state to the ground state are governed not only by the energy gap but also by the nature of the substituents, which presumably affects the changes in the equilibrium displacement or frequency between the two levels. Correlations of the electrochemical redox potentials, the Hammett σ parameter, and the energy of the luminescent level are reported and discussed. Such correlations show that electron-accepting substituents have a larger stabilization effect on the LUMO π* ligand-centered orbital than on the HOMO $\pi(t_{2g})$ metal orbital, whereas electron-donating substituents cause a larger destabilization on the HOMO $\pi(t_{2g})$ metal orbital than on the LUMO π* ligand-centered orbital. Heteroleptic complexes carrying an electron-accepting group and an electron-donating group always show lower emission energies when compared with the parent homoleptic complexes because the π* orbital of the tpy-A ligand is stabilized, and the tpy-D ligand destabilizes the metal-centered $\pi(t_{2g})$ orbitals.

Introduction

The study of the luminescence and redox properties of transition metal complexes is of great interest for a variety of fundamental and practical reasons. In the past 20 years most of the attention in this field has been focused on complexes of the bipyridine-type family (prototype: $[Ru(bpy)_3]^{2+}$, where bpy = 2,2′-bipyridine).[2−4] Such complexes show unique combinations of chemical stability, redox properties, luminescence intensities, and excited state lifetimes. Several hundreds of them have been synthesized and used as photosensitizers in a variety of intermolecular photochemical processes.[2−6]

In recent years it has been realized that the energy and information properties carried by photons will more likely be exploited by photoinduced processes in suitably designed supramolecular (multicomponent) systems rather than in intermolecular photoreactions.[7−13]. The complexes of the $[Ru(bpy)_3]^{2+}$ family have then been used as photosensitizers in covalently-linked multicomponent systems in order to obtain photoinduced migration of electronic energy and/or charge separation.[8,9,13]

An approach to the achievement of such goals is based on the assembly of suitable molecular components (building blocks) according to well-designed structural patterns. As pointed out previously,[14,15] the complexes of the $[Ru(bpy)_3]^{2+}$ family are not suitable from the geometric viewpoint for the construction of supramolecular systems. Therefore, several research groups[15−23] have focused their attention on the complexes of the $[Ru(tpy)_2]^{2+}$ family (tpy = 2,2′:6′,2″-terpyridine) since the tridentate tpy ligand offers several synthetic and structural advantages as compared to the use of the didentate bpy-type ligands. $[Ru(tpy)_2]^{2+}$, however, exhibits less favourable photophysical properties (in particular, lack of luminescence and very short excited state lifetime at room temperature) than $[Ru(bpy)_3]^{2+}$.[23]

⊗ Abstract published in *Advance ACS Abstracts,* April 15, 1995.

(1) (a) Università di Bologna. (b) Universität Basel.
(2) Meyer, T. J. *Pure Appl. Chem.* **1986**, *58*, 1193.
(3) Juris, A.; Balzani, V.; Barigelletti, F.; Campagna, S.; Belser, P.; von Zelewsky, A. *Coord. Chem. Rev.* **1988**, *84*, 85.
(4) Kalyanasundaram, K. *Photochemistry of Polypyridine and Porphyrin Complexes*; Academic Press: London, 1991.
(5) Balzani, V.; Barigelletti, F.; De Cola, L. *Top. Curr. Chem.* **1990**, *158*, 31.
(6) Karvanos, G. J. *Photoinduced Electron Transfer*, VCH Publishers: New York, 1993.
(7) Balzani, V., Ed. *Supramolecular Photochemistry*; Reidel: Dordrecht, The Netherlands, 1987.
(8) Scandola, F.; Indelli, M. T.; Chiorboli, C.; Bignozzi, C. A. *Top. Curr. Chem.* **1990**, *158*, 73.
(9) Balzani, V.; Scandola, F. *Supramolecular Photochemistry*; Horwood: Chichester, England, 1991.
(10) Wasielewski, M. R. *Chem. Rev.* **1992**, *92*, 435.
(11) Gust, D.; Moore, T. A.; Moore, A. L.; *Acc. Chem. Res.* **1993**, *26*, 198.
(12) Bissel, R. A.; de Silva, A. P.; Gunaratne, H. Q. N.; Lynch, P. L. M.; Maguire, G. E. M.; McCoy, C. P.; Sandanayake, K. R. A. S. *Top. Curr. Chem.*, **1993**, *168*, 223.
(13) Balzani, V. Scandola, F. In *Comprehensive Supramolecular Chemistry*, Reinhoudt, D. N., Ed.; Pergamon Press: Oxford, England, Vol. 10, in press.
(14) Collin, J.-P.; Guillerez, S.; Sauvage, J.-P. *J. Chem. Soc., Chem. Commun.*, **1989**, 776.

0020-1669/95/1334-2759$09.00/0

	X	Y
1	$MeSO_2$	$MeSO_2$
2	Cl	Cl
3	H	H
4	Ph	Ph
5	EtO	EtO
6	OH	OH
7	Me_2N	Me_2N
8	H	$MeSO_2$
9	OH	$MeSO_2$
10	Cl	EtO
11	OH	Ph
12	$MeSO_2$	Me_2N
13	Cl	Me_2N
14	OH	Me_2N

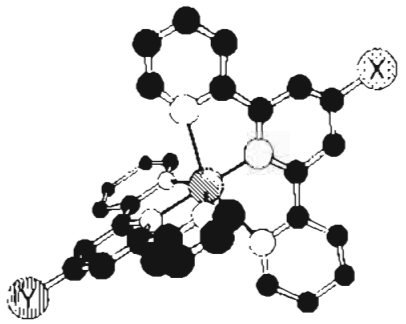

Figure 1. Structural formulas of the $[Ru(tpy\text{-}X)(tpy\text{-}Y)]^{2+}$ complexes.

In a preliminary investigation[24] we showed that suitable substituents in the 4′ position of tpy can yield tpy-type ruthenium(II) complexes which display room temperature luminescence. We have, therefore, decided to carry on a systematic investigation on the effect of varying substituents X and Y in the 4′ position of tpy ligands on the luminescence properties of the resulting $[Ru(tpy\text{-}X)(tpy\text{-}Y)]^{2+}$ complexes[25] (Figure 1). Correlations between excited state energies and electrochemical redox potentials are reported, and the role played by various deactivation processes to determine the excited state lifetime in fluid solution at room temperature and in rigid matrix at 77 K is discussed.

Experimental Section

Absorption spectra were recorded with a Perkin-Elmer lambda 6 spectrophotometer in acetonitrile solution. Luminescence experiments were performed in acetonitrile solution at room temperature and in butyronitrile rigid matrix at 77 K. Corrected luminescence spectra were obtained with a Perkin-Elmer LS 50 spectrofluorimeter. Luminescence lifetimes were obtained with a Edinburgh single photon counting equipment (N_2 lamp, 337 nm). Luminescence quantum yields were measured with a Perkin-Elmer LS 50 spectrofluorimeter, following the method described by Demas and Crosby[26] using $[Ru(bpy)_3]^{2+}$ as a standard ($\Phi = 2.8 \times 10^{-2}$ in aerated water).[27]

^{1}H-NMR spectra were recorded on a Brüker WM250 spectrometer. Fast atom bombardment (FAB) mass spectra were recorded on a Kratos MS-890 spectrometer, using 3-nitrobenzyl alcohol as matrix. Electrochemical measurements were performed using an AMEL Model 553 potentiostat, Model 567 function generator and Model 721 integrator connected to an X-Y recorder *via* an AMEL Model 560/A interface. A conventional three-electrode configuration was used, with platinum bead working and auxiliary electrodes and an Ag/Ag^+ reference. Acetonitrile, freshly distilled from P_4O_{10}, was used as solvent in all cases. The base electrolyte was 0.1 M $[^nBu_4N][BF_4]$, recrystallized twice from ethanol/water and thoroughly dried. Potentials are quoted *vs* the ferrocene/ferrocenium couple ($Fc/Fc^+ = 0.0V$), and all potentials were referenced to internal ferrocene added at the end of each experiment. Elemental analyses were performed at the University Chemical Laboratory, Cambridge, England.

Hydrated ruthenium(III) chloride was used as supplied by Johnson Matthey. The ligands 2,2′:6′,2″-terpyridine (tpy)[28] and 4′-(methylsulfonyl)-2,2′:6′,2″-terpyridine (tpy-SO_2Me)[32] were prepared by the literature methods, while 4′-hydroxy-2,2′:6′,2″-terpyridine (tpy-OH),[30] 4′-chloro-2,2′:6′,2″-terpyridine (tpy-Cl),[30] 4′-phenyl-2,2′:6′,2″-terpyridine (tpy-Ph),[31] 4′-ethoxy-2,2′:6′,2″-terpyridine (tpy-OEt),[25] and 4′-(*N*,*N*-dimethylamino)-2,2′:6′,2″-terpyridine (tpy-NMe_2)[25] were prepared as previously reported. The ruthenium(III) intermediates $[Ru(tpy\text{-}X)Cl_3]$ (X = H, Cl, HO, Me_2N, Ph) were prepared as previously reported.[25] We have reported the syntheses of the homoleptic complexes $[Ru(tpy\text{-}X)_2][PF_6]_2$ (tpy-X = 4′-substituted-2,2′:6′,2″-terpyridine; X = Cl, H, OH, Me_2N, EtO, Ph) elsewhere.[25] All complexes were recrystallized from acetone–methanol solution.

$[Ru(tpy\text{-}SO_2Me)Cl_3]$. 4′-Methylsulfonyl-2,2′:6′,2″-terpyridine (700 mg, 2.25 mmol) was added to $RuCl_3{\cdot}3H_2O$ (540 mg, 2.25 mmol) in ethanol (25 cm^3), and this suspension was heated to reflux for 1 h. The mixture was cooled, and the dark brown precipitate was collected by filtration, washed thoroughly with methanol, water, and ether, and dried *in vacuo* to yield $[Ru(tpy\text{-}SO_2Me)Cl_3]$ (1.16 g, 99%).

$[Ru(tpy\text{-}SO_2Me)_2][PF_6]_2$. 4′-Methylsulfonyl-2,2′:6′,2″-terpyridine (60 mg, 0.193 mmol) was added to $[Ru(tpy\text{-}SO_2Me)Cl_3]$ (100 mg, 0.193 mmol) in methanol (10 cmm3), along with *N*-ethylmorpholine (5 drops). The mixture was heated to reflux for two hours. The resulting deep red solution was filtered through celite and excess methanolic ammonium hexafluorophosphate was added to precipitate $[Ru(tpy\text{-}SO_2Me)_2][PF_6]_2$. This was collected by filtration, recrystallized from actone–methanol solution, and dried *in vacuo* to yield $[Ru(tpy\text{-}SO_2Me)_2][PF_6]_2$ as a red powder (70 mg, 36%). Anal. Calcd for $RuC_{32}H_{26}N_6S_2O_4P_2F_{12}$: C, 37.9; H, 2.6; N, 8.3. Found: C, 37.8; H, 2.6; N, 8.2. FAB: *m/z* 869 (869) $\{[Ru(tpy\text{-}SO_2Me)_2][PF_6]\}^+$, 724 (724) $\{[Ru(tpy\text{-}SO_2Me)_2]\}^+$, 413 (413) $\{[Ru(typ\text{-}SO_2Me)]\}^+$.

$[Ru(tpy)(tpy\text{-}SO_2Me)][PF_6]_2$. A suspension of 4′-(methylsulfonyl)-2,2′:6′,2″-terpyridine (106 mg, 0.341 mmol), $[Ru(tpy)Cl_3]$ (150 mg, 0.341 mmol), and *N*-ethylmorpholine (5 drops) in methanol (20 cm^3) was heated at reflux for 2 h. The resulting deep red solution was filtered through Celite, and excess methanolic ammonium hexafluorophosphate was added to precipitate crude $[Ru(tpy)(tpy\text{-}SO_2Me)][PF_6]_2$. This was collected by filtration, redissolved in the minimum volume of acetonitrile, and chromatographed on a short silica column using acetonitrile, saturated aqueous potassium nitrate, and water (7:1:0.5 v/v) as the

(15) Constable, E. C.; Cargill Thompson, A. M. W. *J. Chem. Soc., Dalton Trans.* **1992**, 3467. Constable, E. C.; Cargill Thompson, A. M. W.; Tocher, D. A. In *Supramolecular Chemistry*, Balzani, V.; De Cola, L., Eds.; Kluwer: Dordrecht, The Netherlands, 1992; p 219. Constable, E. C.; Cargill Thompson, A. M. W. *J. Chem. Soc., Chem. Commun.* **1992**, 617; *J. Chem. Soc., Dalton Trans.* **1992**, 2947. Constable, E. C.; Cargill Thompson, A. M. W.; Tocher, D. A. *Supramol. Chem.* **1993**, *3*, 9; *Polymer Prepr.* **1993**, *34*, 110; *Makromol. Symp.* **1994**, *77*, 219. Newkome, G. R.; Cardullo, F.; Constable, E. C.; Moorefield, C. N.; Cargill Thompson, A. M. W. *J. Chem. Soc., Chem. Commun.* **1993**, 925. Constable, E. C.; Edwards, A. J.; Martínez-Máñez, R.; Raithby, P. R.; Cargill Thompson, A. M. W. *J. Chem. Soc., Dalton Trans.* **1994**, 645. Constable, E. C.; Harverson, P.; Smith, D. R.; Whall, L. A. *Tetrahedron* **1994**, *50*, 7799.
(16) Kober, E. M.; Marshall, J. L.; Dressick, W. J.; Sullivan, B. P.; Caspar, J. V.; Meyer, T. J. *Inorg. Chem.* **1985**, *24*, 2755.
(17) Hecker, C. R.; Gushurst, A. K. I.; McMillin, D. R. *Inorg. Chem.* **1991**, *30*, 538.
(18) Amouyal, E.; Mouallem-Bahout, M.; Calzaferri, G. *J. Phys. Chem.* **1991**, *95*, 7641.
(19) Arana, C. R.; Abruña, H. D. *Inorg. Chem.* **1993**, *32*, 194.
(20) Collin, J.-P.; Guillerez, S.; Sauvage, J.-P.; Barigelletti, F.; De Cola, L.; Flamigni, L.; Balzani, V. *Inorg. Chem.* **1991**, *30*, 4230. Collin, J.-P.; Guillerez, S.; Sauvage, J.-P.; Barigelletti, F.; De Cola, L.; Flamigni, L.; Balzani, V. *Inorg. Chem.* **1992**, *31*, 4112.
(21) Grosshenny, V.; Ziessel, R. *J. Chem. Soc., Dalton Trans.* **1993**, 817. *J. Organomet. Chem.* **1993**, *453*, C19.
(22) Barigelletti, F.; Flamigni, L.; Balzani, V.; Collin, J.-P.; Sauvage, J.-P.; Sour, A.; Constable, E. C.; Cargill Thompson, A. M. W. *J. Chem. Soc., Chem. Commun.*, **1993**, 942. Barigelletti, F.; Flamigni, L.; Balzani, V.; Collin, J.-P.; Sauvage, J.-P.; Sour, A.; Constable, E. C.; Cargill Thompson, A. M. W. *J. Am. Chem. Soc.* **1994**, *116*, 7692.
(23) Sauvage, J.-P.; Collin, J.-P.; Chambron, J.-C.; Guillerez, S.; Coudret, C.; Balzani, V.; Barigelletti, F.; De Cola, L.; Flamigni, L. *Chem. Rev.* **1994**, *94*, 993.
(24) Constable, E. C.; Cargill Thompson, A. M. W.; Armaroli, N.; Balzani, V.; Maestri, M. *Polyhedron* **1992**, *20*, 2707.
(25) Constable, E. C.; Cargill Thompson, A. M. W.; Tocher, D. A.; Daniels, M. A. M. *New J. Chem.* **1992**, *16*, 855.
(26) Demas, J. N.; Crosby, G. A. *J. Phys. Chem.* **1971**, *75*, 991.
(27) Nakamaru, K. *Bull. Chem. Soc. Jpn.* **1982**, *55*, 2697.
(28) Jameson, D. L.; Guise, L. E. *Tetrahedron* **1991**, *32*, 1999.
(29) Potts, K. T.; Cipullo, M. J., Ralli, P.; Theodoridis, G. *J. Org. Chem.* **1982**, *47*, 3027.
(30) Constable, E. C.; Ward, M. D. *J. Chem. Soc., Dalton Trans.* **1990**, 1405.
(31) Constable, E. C., Lewis, J.; Liptrot, M. C., Raithby, P. R. *Inorg. Chim. Acta* **1990**, *178*, 47.
(32) Constable, E. C.; Cargill Thompson, A. M. W. *J. Chem. Soc., Dalton Trans.* **1994**, 1409.

eluent. The main brown band was collected, excess methanolic ammonium hexafluorophosphate added, and the mixture reduced in volume to induce precipitation. After recrystallization from 1:1 acetone-methanol, $[Ru(tpy)(tpy\text{-}SO_2Me)][PF_6]_2$ was collected as an analytically pure red-brown powder (150 mg, 43%). Anal. Calcd for $RuC_{31}H_{24}N_6O_2SP_2F_{12}$: C, 39.8; H, 2.6; N, 9.0. Found: C, 39.7; H, 2.5; N, 8.9. FAB: *m/z* 791 (791) $\{[Ru(tpy)(tpy\text{-}SO_2Me)][PF_6]_2\}^+$, 646 (646) $\{[Ru(tpy)(tpy\text{-}SO_2Me)]\}^+$.

$[Ru(tpy\text{-}OH)(tpy\text{-}SO_2Me)][PF_6]_2$. A suspension of 4′-(methylsulfonyl)-2,2′:6′,2″-terpyridine (61 mg, 0.196 mmol), $[Ru(tpy\text{-}OH)Cl_3]$ (90 mg, 0.197 mmol), and *N*-ethylmorpholine (5 drops) in methanol (20 cm^3) was heated at reflux for 2 h. The resulting deep red solution was filtered through Celite, and excess methanolic ammonium hexafluorophosphate was added to precipitate crude $[Ru(tpy\text{-}OH)(tpy\text{-}SO_2Me)][PF_6]_2$. This was collected by filtration, redissolved in the minimum volume of acetonitrile, and chromatographed on a short silica column using acetonitrile, saturated aqueous potassium nitrate, and water (7:1:0.5 v/v) as the eluent. The main brown band was collected as a number of fractions, the purity of the fractions being checked by thin-layer chromatography prior to combination. Excess hexafluorophosphoric acid was added to the combined fractions, and the mixture was reduced in volume to induce precipitation. After recrystallization from 1:1 acetone-methanol to which HPF_6 (1 drop) had been added, $[Ru(tpy\text{-}OH)(tpy\text{-}SO_2Me)][PF_6]_2$ was collected as an analytically pure red-brown powder (86 mg, 46%). Anal. Calcd for $RuC_{31}H_{24}N_6O_3SP_2F_{12}$: C, 39.1; H, 2.5; N, 8.8. Found: C, 38.4; H, 2.6; N, 8.4. FAB: *m/z* 808 (807) $\{[Ru(tpy\text{-}OH)(tpy\text{-}SO_2Me)][PF_6]\}^+$, 661 (662) $\{[Ru(tpy\text{-}OH)(tpy\text{-}SO_2Me)]\}^+$.

$[Ru(tpy\text{-}NMe_2)(tpy\text{-}SO_2Me)][PF_6]_2$. A suspension of 4′-methylsulfonyl-2,2′:6′,2″-terpyridine (57 mg, 0.182 mmol), $[Ru(tpy\text{-}NMe_2)Cl_3]$ (88 mg, 0.182 mmol), and *N*-ethylmorpholine (5 drops) in methanol (20 cm^3) was heated at reflux for 2 h. The resulting deep red solution was filtered through Celite and excess methanolic ammonium hexafluorophosphate was added to precipitate crude $[Ru(tpy\text{-}NMe_2)(tpy\text{-}SO_2Me)][PF_6]_2$. This was collected by filtration, redissolved in the minimum volume of acetonitrile, and chromatographed on a short silica column using acetonitrile, saturated aqueous potassium nitrate, and water (7:1:0.5 v/v) as the eluent. The main brown band was collected as a number of fractions, the purity of the fractions being checked by thin-layer chromatography prior to combination. Excess methanolic ammonium hexafluorophosphate was added to the combined fractions, and the mixture was reduced in volume to induce precipitation. After recrystallization from 1:1 acetone−methanol, $[Ru(tpy\text{-}NMe_2)(tpy\text{-}SO_2Me)][PF_6]_2$ was collected as an analytically pure red-brown powder (50 mg, 28%). Anal. Calcd for $RuC_{33}H_{27}N_7O_2SP_2F_{12}$: C, 40.5: H, 2.8; N, 10.0. Found: C, 40.1; H, 2.5; N, 9.8. FAB: *m/z* 835 (834) $\{[Ru(tpy\text{-}NMe_2)(tpy\text{-}SO_2Me)][PF_6]\}^+$, 689 (689) $\{[Ru(tpy\text{-}NMe_2)(tpy\text{-}SO_2Me)]\}^+$.

$[Ru(tpy\text{-}Cl)(tpy\text{-}OEt][PF_6]_2$. 4′-Ethoxy-2,2′:6′,2″-terpyridine (51 mg, 0.20 mmol) was added to $[Ru(tpy\text{-}Cl)Cl_3]$ (87 mg, 0.18 mmol) in methanol (20 cm^3). *N*-Ethylmorpholine (5 drops) was added, and the mixture was heated to reflux for 1 h. The resulting deep red solution was reduced in volume to 3 cm^3 and chromatographed on a short silica column using acetonitrile, saturated aqueous potassium nitrate, and water (7:1:0.5 v/v) as the eluent. The main brown band was collected, excess methanolic ammonium hexafluorophosphate added, and the mixture reduced in volume to induce precipitation. After recrystallization from 1:1 acetone−methanol, $[Ru(tpy\text{-}Cl)(tpy\text{-}OEt)][PF_6]_2$ was collected as a dark red-brown powder (62 mg, 36%), which was washed with a little aqueous methanol and dried *in vacuo*. Anal. Calcd for $RuC_{32}H_{25}N_6OClP_2F_{12}$: C, 41.0; H, 2.7; N, 9.0. Found: C, 40.0; H, 2.5; N, 8.9. FAB: *m/z* 646 (646) $\{[Ru(tpy\text{-}Cl)(tpy\text{-}OEt)]\}^+$, 617 (617) $\{[Ru(tpy\text{-}Cl)(tpy\text{-}OEt)] - Et\}^+$.

$[Ru(tpy\text{-}Cl)(tpy\text{-}NMe_2)][PF_6]_2$. 4′-(*N*,*N*-Dimethylamino)-2,2′:6′,2″-terpyridine (29 mg, 0.11 mmol) was added to $[Ru(tpy\text{-}Cl)Cl_3]$ (50 mg, 0.11 mmol) in methanol (10 cm^3). *N*-Ethylmorpholine (2 drops) was added, and the mixture was heated to reflux for 1 h. The resulting deep red solution was reduced in volume to 3 cm^3 and chromatographed on a short silica column using acetonitrile, saturated aqueous potassium nitrate, and water (7:1:0.5 v/v) as the eluent. The main brown band was collected, excess methanolic ammonium hexafluorophosphate added, and the mixture reduced in volume to induce precipitation. After recrystallization from 1:1 acetone−methanol, $[Ru(tpy\text{-}Cl)(tpy\text{-}NMe_2)][PF_6]_2$ was collected as a brown powder (60 mg, 61%), washed with a little aqueous methanol, and dried *in vacuo*. Anal. Calculated for $RuC_{32}H_{26}N_7ClP_2F_{12}$: C, 41.1; H, 2.8; N, 10.5. Found: C, 40.5; H, 2.7; N, 10.4. FAB: *m/z* 790 (790) $\{[Ru(tpy\text{-}Cl)(tpy\text{-}NMe_2)][PF_6]\}^+$, 645 (645) $\{[Ru(tpy\text{-}Cl)\ (tpy\text{-}NMe_2)]\}^+$, 630 (630) $\{[Ru(tpy\text{-}Cl)(tpy\text{-}NMe_2)] - Me\}^+$.

$[Ru(tpy\text{-}OH)(tpy\text{-}Ph][PF_6]_2$. 4′-Hydroxy-2,2′:6′,2″-terpyridine (34 mg, 0.14 mmol) was added to $[Ru(tpy\text{-}Ph)Cl_3]$ (70 mg, 0.14 mmol) in methanol (10 cm^3). *N*-Ethylmorpholine (2 drops) was added, and the mixture was heated to reflux for 1 h. The resulting deep red solution was reduced in volume to 3 cm^3 and chromatographed on a short silica column using acetonitrile, saturated aqueous potassium nitrate, and water (7:1:0.5 v/v) as the eluent. The main orange-brown band was collected, excess HPF_6 added, and the mixture reduced in volume to induce precipitation. After recrystallization from 1:1 acetone−methanol, $[Ru(tpy\text{-}OH)(tpy\text{-}Ph][PF_6]_2$ was collected as a red-brown powder (60 mg, 44%) which was washed with a little aqueous methanol and dried *in vacuo*. Anal. Calcd for $RuC_{36}H_{26}N_6OP_2F_{12}$: C, 45.5; H, 2.7; N, 8.9. Found: C, 45.2; H, 2.9; N, 8.6. FAB *m/z* 804 (805) $\{[Ru(tpy\text{-}OH)(tpy\text{-}Ph)][PF_6]\}^+$, 659 (660) $\{[Ru(tpy\text{-}OH)(tpy\text{-}Ph)]\}^+$, 411 (411) $\{[Ru(tpy\text{-}Ph)]\}^+$.

$[Ru(tpy\text{-}OH)(tpy\text{-}NMe_2)][PF_6]_2$. 4′-(*N*,*N*-Dimethylamino)-2,2′:6′,2″-terpyridine (30 mg, 0.11 mmol) was added to $[Ru(tpy\text{-}OH)Cl_3]$ (50 mg, 0.11 mmol) in methanol (10 cm^3). *N*-Ethylmorpholine (2 drops) was added, and the mixture was heated to reflux for 1 h. The resulting deep red solution was reduced in volume to 3 cm^3 and chromatographed on a short silica column using acetonitrile, saturated aqueous potassium nitrate, and water (7:1:0.5 v/v) as the eluent. The main orange-brown band was collected, excess HPF_6 added, and the mixture reduced in volume to induce precipitation. After recrystallization from 1:1 acetone−methanol, $[Ru(tpy\text{-}OH)(tpy\text{-}NMe_2)][PF_6]_2$ was collected as a brown powder (43 mg, 43%), washed with a little aqueous methanol and dried *in vacuo*. Anal. Calcd for $RuC_{32}H_{27}N_7OP_2F_{12}$: C, 41.9; H, 2.9; N, 10.7. Found: C, 41.6; H, 2.9; N, 10.6. FAB: *m/z* 626 (627) $\{[Ru(tpy\text{-}OH)(tpy\text{-}NMe_2)]\}^+$, 610 (610) $\{[Ru(tpy\text{-}OH)(tpy\text{-}NMe_2)]\text{-}OH\}^+$.

Results

Synthesis. The investigated complexes have the structural formulas shown in Figure 1. The X and Y substituents which have been used to obtain the various complexes are also shown.

Ruthenium(II)−bis(2,2′:6′,2″-terpyridine) species are conveniently prepared by the stepwise addition of the two terpyridine ligands to the ruthenium center.[25] The reaction of equimolar quantities of tpy-X and hydrated ruthenium trichloride at reflux in ethanol affords a dark brown insoluble $[Ru(tpy\text{-}X)Cl_3]$ species. This is then reacted with 1 equiv of either the same terpyridine (tpy-X) or else another (tpy-Y) at reflux in methanol, in the presence of *N*-ethylmorpholine as a reducing agent, to give homoleptic $[Ru(tpy\text{-}X)_2]^{2+}$ or heteroleptic $[Ru(tpy\text{-}X)(tpy\text{-}Y)]^{2+}$, respectively. These complexes are readily precipitated as hexafluorophosphate salts by the addition of excess methanolic $[NH_4][PF_6]$ (or HPF_6 if the ligand 4′-hydroxy-2,2′:6′,2″-terpyridine (tpy-OH) is present in order to ensure that it is not in the deprotonated tpy-O^- form).[25] The homoleptic complexes were recrystallized from 1:1 acetone−methanol solution and obtained as analytically pure intensely colored powders. ^1H-NMR studies of CD_3CN solutions showed the heteroleptic $[Ru(tpy\text{-}X)(tpy\text{-}Y)][PF_6]_2$ species to be contaminated with small amounts of the homoleptic parent species $[Ru(tpy\text{-}X)_2][PF_6]_2$ and $[Ru(tpy\text{-}Y)_2][PF_6]_2$. These impurities could be removed by chromatography on a silica column using acetonitrile, saturated aqueous potassium nitrate, and water (7:1:0.5 v/v) as eluent. The main product fraction was collected and anion metathesis with $[NH_4][PF_6]$ (or HPF_6) performed, followed by recrystallization from 1:1 acetone−methanol, to give the product as an analytically pure powder.

Table 1. ^{1}H NMR Data (δ, CD_3CN Solution) for the $[Ru(tpy\text{-}X)(tpy\text{-}Y)](PF_6)_2$ Complexes

	X	Y	3 4H d	4 4H dd	5 4H dd	6 4H d	3′ 4H s	
1	$MeSO_2$	$MeSO_2$	8.68	7.98	7.23	7.40	9.15	Me 3.52, 6H s
2	Cl	Cl	8.47	7.94	7.19	7.39	8.84	
3	H	H	8.48	7.91	7.15	7.33	8.74 d	4′ 8.40, 2H t
4	Ph	Ph	8.64	7.95	7.18	7.43	9.01	o 8.21, 4H d; m + p 7.75, 6H m
5	EtO	EtO	8.46	7.88	7.13	7.37	8.27	CH_2 4.58, 4H q; CH_3 1.64, 6H t
6	HO	HO	8.38	7.87	7.14	7.39	8.18	
7	Me_2N	Me_2N	8.45	7.83	7.11	7.37	7.91	Me 3.44, 12H s

	X	Y	3 2H d	4 2H dd	5 2H dd	6 2H d	3′ 2H s		3 2H d	4 2H dd	5 2H dd	6 2H d	3′ 2H s	
8	H	$MeSO_2$	8.67	7.97	7.24	7.41	9.12	Me 3.50, 3H s	8.48	7.93	7.13	7.32	8.77 d	4′ 8.48, 1H t
9	HO	$MeSO_2$	8.66	7.97	7.28	7.50	9.10	Me 3.49, 3H s	8.40	7.89	7.09	7.26	8.23	
10[a]	Cl	EtO	8.89	8.11	7.40	7.85	9.18		8.84	8.06	7.29	7.75	8.71	CH_2 4.69, 2H q; CH_3 1.65, 3H t
11	HO	Ph	8.41	7.90	7.13	7.37	8.22		8.63	7.95	7.21	7.47	8.99	o 8.20, 2H d; m + p 7.75, 3H m
12	$MeSO_2$	Me_2N	8.66	7.96	7.30	7.55	9.08	Me 3.48, 3H s	8.48	7.86	7.03	7.18	7.94	Me 3.48, 6H s
13[a]	Cl	Me_2N	8.89	8.11	7.45	7.88	9.16		8.83	8.00	7.22	7.66	8.36	Me 3.59, 6H s
14	HO	Me_2N	8.39	7.87	7.09	7.43	8.18		8.47	7.87	7.17	7.34	7.92	Me 3.46, 6H s

[a] Spectrum obtained for a CD_3COCD_3 solution.

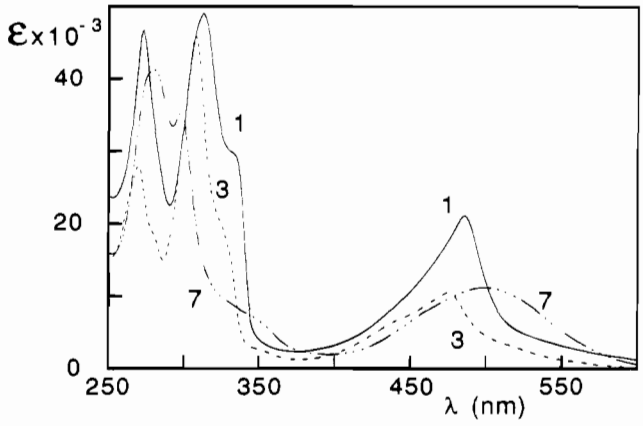

Figure 2. Absorption spectra of $[Ru(tpy)_2]^{2+}$ (**3**), $[Ru(tpy\text{-}SO_2Me)_2]^{2+}$ (**1**), and $[Ru(tpy\text{-}NMe_2)_2]^{2+}$ (**7**) in acetonitrile solution at room temperature.

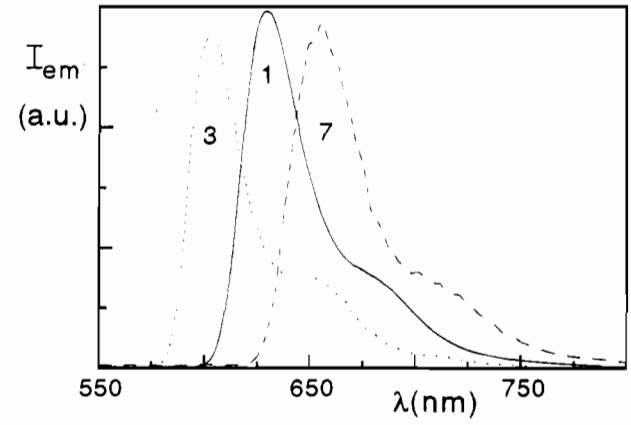

Figure 3. Luminescence spectra of $[Ru(tpy)_2]^{2+}$ (**3**), $[Ru(tpy\text{-}SO_2Me)_2]^{2+}$ (**1**), and $[Ru(tpy\text{-}NMe_2)_2]^{2+}$ (**7**) in butyronitrile rigid matrix at 77 K.

^{1}H-NMR spectra (Table 1) were recorded for CD_3CN (or CD_3COCD_3) solutions of the complexes. The solution species are highly symmetrical, with only five or six pyridine ring resonances (along with any resonances arising from the substituent group) being observed for the homoleptic $[Ru(tpy\text{-}X)_2][PF_6]_2$ species. As we have commented on elsewhere, the ^{1}H-NMR spectra of solutions of heteroleptic $[Ru(tpy\text{-}X)(tpy\text{-}Y)][PF_6]_2$ species are similar to superimposition of the spectra of the homoleptic parent species $[Ru(tpy\text{-}X)_2][PF_6]_2$ and $[Ru(tpy\text{-}Y)_2][PF_6]_2$.[25]

Absorption Spectra. The absorption spectrum of the prototype $[Ru(tpy)_2]^{2+}$ (**3**) complex and of the $[Ru(tpy\text{-}SO_2Me)_2]^{2+}$ (**1**) and $[Ru(tpy\text{-}NMe_2)_2]^{2+}$ (**7**) derivatives are shown in Figure 2 (all as the $[PF_6]^-$ salts). The wavelength of the maximum of the lowest energy absorption band of all the complexes investigated is shown in Table 2. As exemplified by the spectra shown in Figure 2, the ligand-centered bands of the aromatic tpy structure are considerably shifted to shorter wavelengths by the presence of electron donating substituents in the 4′ position, whereas electron-accepting substituents have a much smaller bathochromic effect. The spin-allowed metal-to-ligand charge-transfer (^{1}MLCT) band in the visible spectral region undergoes an increase in intensity and a red shift, regardless of the electron-donor or electron-acceptor nature of the substituents.

Luminescence Properties. It is well-known[2-6] that the excited state responsible for the luminescence of the Ru(II)-polypyridine compounds is the lowest triplet metal-to-ligand charge-transfer (^{3}MLCT) excited state. The luminescence data have been gathered in Table 2. At room temperature most of the complexes exhibit a luminescence quantum yield higher than that of $[Ru(tpy)_2]^{2+}$ and a longer excited state lifetime. For the homoleptic complexes containing strong electron-donating ligands, no luminescence can be observed. In all cases in which luminescence has been recorded, a considerable red shift of the emission maximum is observed compared with that of $[Ru(tpy)_2]^{2+}$.

In rigid matrix at 77 K, all of the complexes exhibit a strong luminescence, again red shifted compared with that of $[Ru(tpy)_2]^{2+}$. The luminescence spectra of $[Ru(tpy)_2]^{2+}$ (**3**), $[Ru(tpy\text{-}SO_2Me)_2]^{2+}$ (**1**), and $[Ru(tpy\text{-}NMe_2)_2]^{2+}$ (**7**) are shown in Figure 3. The excited state lifetime in most cases is shorter than that of $[Ru(tpy)_2]^{2+}$. For some representative complexes, the change in the excited state lifetime with change of temperature has been investigated (Figure 4). The data obtained are shown in Table 3.

Electrochemical Behavior. For all the complexes examined, the first oxidation wave and the first reduction wave are reversible. The $E_{1/2}$ values for these processes are shown in Table 2.

Discussion

The data collected in Table 2 show that substitution of electron-donating (D) or electron-accepting (A) groups in the

Table 2. Photophysical Properties and Redox Potentials of $[Ru(tpy\text{-}X)(tpy\text{-}Y)](PF_6)_2$ Complexes

			abs 298 K[a]		em 298 K[a]			em 77 K[b]		electrochemistry[c]		
	X	Y	λ (nm)[e]	ϵ (M^{-1} cm^{-1})	λ (nm)[f]	τ (ns)[g]	Φ_{em}[h]	λ (nm)[f]	τ (μs)[g]	E_{red} (V)	E_{ox} (V)	σ[d]
1	$MeSO_2$	$MeSO_2$	486	21 100	666	25.0	5×10^{-4}	632	11.3	−1.34	1.10	0.73
2	Cl	Cl	480	17 000	653	0.2	$\leq 1 \times 10^{-5}$	616	8.9	−1.53	1.00	0.24
3	H	H	474	10 400	629		$\leq 5 \times 10^{-6}$	598	10.6	−1.67	0.92	0.00
4	Ph	Ph	487	26 200	715	1.0	4×10^{-5}	629	11.9	−1.66	0.90	−0.01
5	EtO	EtO	485	16 500				621	6.8	−1.76	0.74	−0.24
6	OH	OH	484	14 500				620	6.6	−1.81	0.73	−0.38
7	Me_2N	Me_2N	499	11 200				657	5.4	−1.90	0.42	−0.83
8	H	$MeSO_2$	482	17 700	679	36.0	4×10^{-4}	642	11.1	−1.40	1.02	
9	OH	$MeSO_2$	490	16 800	706	50.0	5×10^{-4}	659	6.4	−1.53	0.92	
10	Cl	EtO	484	16 600	668	0.2	$\leq 1 \times 10^{-5}$	626	7.6	−1.57	0.85	
11	OH	Ph	488	17 000	675	0.4	1×10^{-5}	637	10.0	−1.82	0.81	
12	$MeSO_2$	Me_2N	500	18 800	~800			723	1.5	−1.47	0.66	
13	Cl	Me_2N	497	16 200	746		$\leq 1 \times 10^{-5}$	669	2.3	−1.64	0.61	
14	OH	Me_2N	494	14 800				657	5.0	−1.86	0.50	

[a] Acetonitrile. [b] Butyronitrile. [c] Acetonitrile, V vs Fc/Fc^+, all reversible; most of the data are taken from ref 25. [d] Hammett σ parameter values; from ref 39. [e] Wavelength of the lowest energy absorption maximum. [f] Wavelength of highest energy emission feature. [g] Luminescence emission lifetime (±10%). [h] Luminescence quantum yield (±20%).

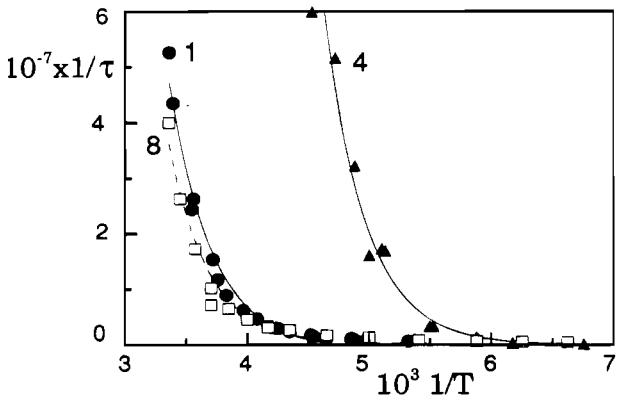

Figure 4. Temperature dependence of the luminescence lifetime for $[Ru(tpy\text{-}SO_2Me)_2]^{2+}$ (**1**), $[Ru(tpy\text{-}Ph)_2]^{2+}$ (**4**), and $[Ru(tpy)(tpy\text{-}SO_2Me)]^{2+}$ (**8**).

Table 3. Parameters from the Temperature-Dependent Lifetime Data[a]

	X	Y	ΔE_1 (cm^{-1})	$A_1 \times 10^{-13}$ (s^{-1})
1	$MeSO_2$	$MeSO_2$	2600	1.3
3[b]	H	H	1500	1.9
4	Ph	Ph	2000	5.4
6[c]	OH	OH	<1000	
7[d]	Me_2N	Me_2N	<600	
8	H	$MeSO_2$	2800	3.3
e	CH_3Ph	CH_3Ph	1800	1.5

[a] Butyronitrile solutions; eq 4. [b] From ref 17. [c] No emission above 200 K. [d] No emission above 170 K. [e] F. Barigelletti private communication.

4′ position of the tpy ligand causes dramatic changes in the properties of the Ru(II)-tpy complexes. In particular, two general, and at a first sight conflicting, trends clearly emerge. Compared with the parent $[Ru(tpy)_2]^{2+}$ complex, (i) the energy of the emission maximum decreases regardless of the electron-accepting or electron-donating nature of the substituents, and (ii) at high temperature, electron-accepting substituents increase the luminescence quantum yield and the excited state lifetime, whereas electron-donating substituents have an opposite effect. In an attempt to rationalize these results, we will now examine correlations between spectroscopic, photophysical, and electrochemical data.

Correlation between Excited State Energies and Redox Potentials. It is well known that in Ru(II)−polypyridine complexes (i) oxidation is metal centered, (ii) reduction is ligand centered, and (iii) the lowest energy absorption band and the luminescence band have a MLCT orbital origin.[2-6] On the assumption that the $\pi(t_{2g})$ metal orbital involved in the oxidation process and the ligand π^* orbital involved in the first reduction process are also the orbitals involved in the MLCT absorption and emission processes, the following linear correlations are expected[33]

$$h\nu_{abs} = a + b\Delta E_{1/2} \quad (1)$$

$$h\nu_{em} = a' + b'\Delta E_{1/2} \quad (2)$$

between the energy of the absorption (or emission) maximum and the quantity

$$\Delta E_{1/2} = [E_{1/2}Ru(tpy\text{-}X)(tpy\text{-}Y)^{3+/2+}] - [E_{1/2}Ru(tpy\text{-}X)(tpy\text{-}Y)^{2+/+}]$$

which is a measure of the energy difference between the two orbitals involved in the MLCT transition.[3,34-37]

The plots obtained are shown in Figure 5. The general trend indeed shows an increase in the absorption and emission energies with increasing $\Delta E_{1/2}$, which confirms the MLCT nature of the luminescent excited state for all the complexes of this series. The points, however, are relatively scattered, indicating that the specific properties of the various complexes play a role. In the case of absorption, several bands probably overlap, so the possibility should be considered that in some cases the energy of the band maximum does not correspond to

(33) Rillema, D. P.; Allen, G.; Meyer, T. J.; Conrad, D. *Inorg. Chem.* **1983**, *22*, 1617.
(34) The constants *a* and *b* or *a′* and *b′* embody several factors including the Coulombic terms which account for differences caused by a Ru(II) or Ru(III) core, the different solvation of ground states, excited states, reduced and oxidized products, changes in electronic repulsion in the ground and triplet or singlet excited states, differences in vibrational coordinates in going from ground to excited state. Such factors are, of course, influenced by the presence of substituents. Clearly, any interpretation of the spectroscopic and electrochemical results based on the values of the parameters of eqs 1 and 2 is hopeless.
(35) Ohsawa, Y.; Hanck, K. W.; De Armond, M. K. *J. Electroanal. Chem.* **1984**, *175*, 229.
(36) Dodsworth, E. S.; Lever, A. B. P. *Chem. Phys. Lett.* **1986**, *124*, 152.
(37) Barigelletti, F.; Juris, A.; Balzani, V.; Belser, P.; von Zelewsky, A. *Inorg. Chem.* **1987**, *26*, 4115.
(38) A somewhat similar trend has previously been observed upon 4 and 4,4′ substitution of the bpy ligands of $Ru(bpy)_3^{2+}$: Cook, M. J.; Lewis, A. P.; McAuliffe, G. S. G.; Skarda, V.; Thomson, A. J. *J. Chem. Soc., Perkin Trans. 2*, **1984**, 1293.

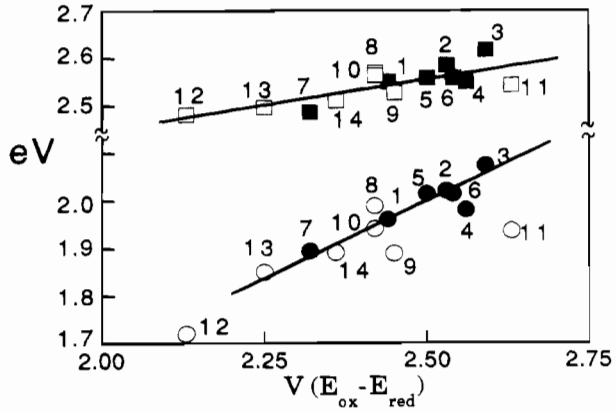

Figure 5. Correlation between the energy of the absorption maximum (squares) and emission maximum at 77 K (circles) and the redox energy $\Delta E_{1/2} = V(E_{ox} - E_{red})$. Solid and open symbols refer to homoleptic and heteroleptic complexes, respectively. For emission, the regression has been performed using only the data concerning the homoleptic complexes. Absorption: slope, 0.22; intercept 1.71, correlation coefficient, 0.783. Emission: slope, 0.64; intercept, 0.41; correlation coefficient, 0.985.

the lowest energy ^{1}MLCT transition. As far as emission is concerned, the plot of Figure 5 shows that the homoleptic complexes are well behaved, with the exception of $[Ru(tpy\text{-}Ph)_2]^{2+}$ (**4**). Among the more scattered data of the heteroleptic complexes, the most anomalous one seems to be that for $[Ru(tpy\text{-}OH)(tpy\text{-}Ph)]^{2+}$ (**11**). We will see later that the complexes of the tpy-Ph ligand also exhibit unusual behavior in other respects.

The data gathered in Table 2 show that *all* the $[Ru(tpy\text{-}X)(tpy\text{-}Y)]^{2+}$ complexes emit at lower energy than $[Ru(tpy)_2]^{2+}$, *regardless of the electron-donating or -accepting nature of the substituents*.[38] This result is clearly illustrated in the diagrams of Figure 6 where the energy of the emission maximum at 77 K is plotted against the potentials of the oxidation and reduction processes. In order to elucidate this somewhat surprising result, we will first discuss the plots of Figure 7 where the potentials of the oxidation and reduction processes of the homoleptic complexes are reported against the Hammett σ parameter.[39] Such plots show that (i) electron-accepting substituents, as expected for proximity reasons, stabilize the LUMO π^* ligand orbital more than the HOMO $\pi(t_{2g})$ metal orbital and (ii) the electron-donor groups destabilize the HOMO $\pi(t_{2g})$ metal orbital more than the LUMO π^* ligand orbital. The latter effect, at first sight surprising since it contradicts the expectation based on proximity, can be understood considering that removal of one electron from the metal causes the formation of Ru^{3+} which withdraws electronic charge from the two tpy-D ligands destabilizing the HOMO $\pi(t_{2g})$ metal orbitals.

We can now go back to discuss the results shown in Figure 6. Consider, first, the homoleptic complexes. With the exception of $[Ru(tpy\text{-}Ph)_2]^{2+}$, starting with the complex which carries the more powerful electron-donating group the energy of the luminescent level increases linearly as the potential of the reduction process decreases and the potential of the oxidation process increases. But as soon as H is replaced by electron-accepting groups, the trend is reversed. It can also be noticed that in the plot against the potential of the oxidation process the (positive) slope for the electron-donating substituents is less steep than the (negative) slope for the electron-accepting substituents, whereas the reverse is true in the plot against the reduction potential. These results parallel the previously discussed correlations (Figure 7) between redox potentials and Hammett σ parameter. More specifically, the decrease of the excited state energy regardless of the electron-donating or -accepting nature of the substituents can be explained considering the MLCT nature of the excited state (Figure 8). When the substituents are electron accepting groups, the π^* ligand-centered orbital is more stabilized than the $\pi(t_{2g})$ metal-centered orbital for proximity reasons, and the oxidized (in the excited state) metal does not receive any charge compensation from the tpy-A ligand not involved in the electronic transition because of the presence of the electron-accepting substituent. When the substituents are electron-donating groups, the MLCT excited state energy decreases as a consequence of the larger destabilization of the metal-centered $\pi(t_{2g})$ orbital compared with the ligand-centered π^* orbital, due to the charge donated to the Ru^{3+} ion by the tpy-D ligand not involved in the MLCT transition. Note that the destabilization effect on $\pi(t_{2g})$ orbitals occurs only when the metal is oxidized, i.e. in $[Ru(tpy\text{-}D)_2]^{3+}$ species and in the MLCT excited state of $[Ru(tpy\text{-}D)_2]^{2+}$.

The fact that heteroleptic complexes carrying an electron-accepting and an electron-donating group always show lower emission energies than the parent homoleptic complexes (Figure 6) can now be easily explained. The π^* orbital of the tpy-A ligand is stabilized because of the presence of the electron-accepting group and becomes the LUMO orbital. At the same time, the tpy-D ligand destabilizes the HOMO metal-centered $\pi(t_{2g})$ orbital. In other words, both substituents concur to lower the excited state energy (Figure 8). As one can see, linear correlations can also be found in Figure 6 within certain sub-families. For example, for X = $MeSO_2$ the emission energy decreases linearly as the oxidation potential becomes less positive along the sub-family Y = $MeSO_2$, H, OH, Me_2N (**1**, **8**, **9**, **12**).

$[Ru(tpy\text{-}Ph)_2]^{2+}$ (**4**) does not follow the linear relationships of the other homoleptic complexes in the spectroscopic/electrochemical plots of Figure 6. From the viewpoint of the Hammett σ parameter Ph is substantially the same as H, as is also shown by its behavior in the plot of Figure 7. Therefore, there must be some peculiarity which causes the emission energy to be smaller than expected. In other words, the luminescent excited state is somewhat stabilized compared with the electrochemical expectations. This effect could be related to the dihedral angle between the plane of the tpy ligand and that of the Ph substituent, which could have different values in the ground state and in the excited state (and also in the oxidized and reduced species). The data would suggest a relaxation of the excited state toward a structure which stabilizes the charge separation created by light excitation.

Correlations between Energy and Lifetime of the Luminescent Excited State. The decay of excited states takes place by competitive radiative and radiationless transitions. For ^{3}MLCT excited states of polypyridine complexes the decay can usually be expressed by the following equation[3]

$$1/\tau = k^r + k_a^{nr} + k_b^{nr}(T) \qquad (3)$$

where τ is the excited state lifetime, k^r is the radiative rate constant and k_a^{nr} and $k_b^{nr}(T)$ are temperature independent and temperature dependent nonradiative rate constants. The temperature dependence of the excited state lifetime of Ru(II)–

(39) Perrin, D. D.; Dempsey, B.; Serjeant, E. P. *pK$_a$ Prediction for Organic Acids and Bases*, Chapman and Hall: London, 1981. Previously reported correlations[32] used the σ^+ parameter, but with this more extensive series of compounds we have reverted to the more accessible σ values.

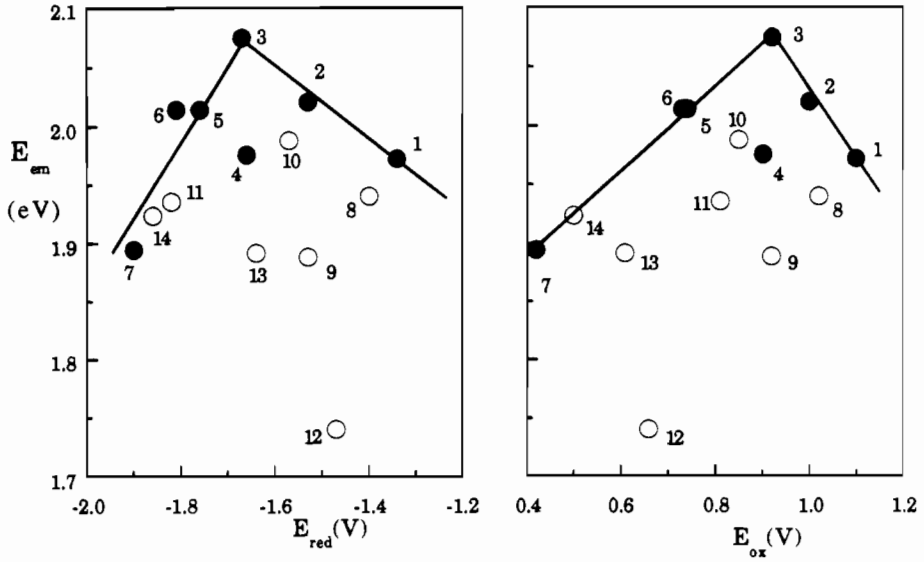

Figure 6. Plot of the emission energy (77 K) *vs* the potentials of the reduction and oxidation processes. Key: solid circles, homoleptic complexes; open circles, heteroleptic complexes.

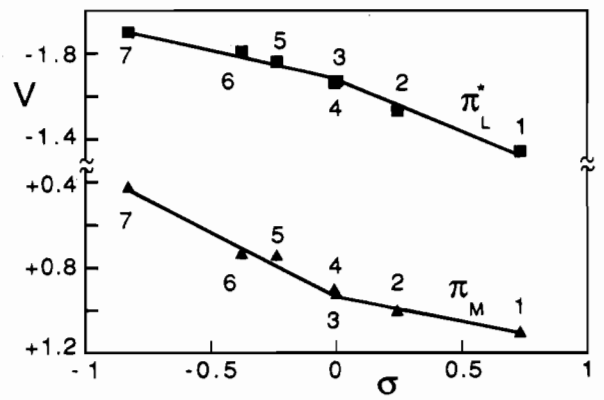

Figure 7. Potentials of the oxidation (triangles) and reduction (squares) processes of the homoleptic complexes as a function of the Hammett σ parameter.

polypyridine complexes usually fits the equation[3]

$$1/\tau = A_o + B_i/(1 + \exp[C_i(1/T - 1/T_{Bi})]) + A_1 e^{-\Delta E_1/RT} \quad (4)$$

where A_o is the lifetime at 77 K. Comparison with eq 3 shows that $A_o = k^r + k_a^{nr}$ and $B_i/(1 + \exp[C_i(1/T - 1/T_{Bi})]) + A_1 e^{-\Delta E_1/RT} = k_b^{nr}(T)$. The $B_i/(1 + \exp[C_i(1/T - 1/T_{Bi})])$ term can be associated to the decrease of lifetime on passing from rigid matrix to fluid solution, whereas the $A_1 e^{-\Delta E_1/RT}$ term can be associated with an activated surface crossing to an upper lying level (*vide infra*).[3] From the quantum yield data collected in Table 2, it is clear that the decay of the luminescent excited state at room temperature is dominated by radiationless transitions. The radiative rate constant, obtained from the relationship $\eta\Phi = k_r\tau$ is in fact of the order of 10^4 s^{-1} (in the reasonable assumption that η, the quantum efficiency for reaching the emitting state, is 1). Comparison with the values of excited state lifetime (Table 2) shows that radiationless decay dominates even at 77 K. Therefore, $k_a^{nr} \sim 1/\tau$ (77 K).

High Temperature Radiationless Decay. As temperature increases, the $A_1 e^{-\Delta E_1/RT} = k_b^{nr}(T)$ term becomes important (Figure 4). At room temperature, it represents by far the predominant radiationless decay path. This behavior, which is quite general for Ru(II)−polypyridine compounds, can be interpreted as an activated surface crossing to an upper lying, shorter lived ^{3}MC (metal-centered) level which derives from a $\pi(t_{2g}) \rightarrow {}^*\sigma(e_g)$ transition.[40-42] As developed in more detail elsewhere,[3] the ΔE_1 activation energy values obtained from the best fitting of the experimental points shown in Figure 4 may represent either the energy gap between the ^{3}MLCT and ^{3}MC level or the distance between the ^{3}MLCT level and the crossing point of the two surfaces. For complexes of the same family the ΔE_1 data have probably the same meaning and the energy gap between the minimum energy of the ^{3}MLCT and ^{3}MC level is most likely related to the distance between the ^{3}MLCT level and the crossing point of the two surfaces. In such a case the data shown in Table 3 indicate that the energy gap between the luminescent ^{3}MLCT level and the ^{3}MC level increases on replacing the 4′ H with the electron-accepting $MeSO_2$ substituent, while it decreases when the electron-donating Me_2N group is present. These results can be interpreted on the basis of the orbital energy diagram of Figure 8 assuming that the effect of the substituents on the tpy ligands does not substantially affect the energy of the σ^* metal orbitals.[43] The electron-accepting substituents stabilize the $(\pi(t_{2g}) \rightarrow {}^*\pi_L)$ ^{3}MLCT level and destabilize the $(\pi(t_{2g}) \rightarrow {}^*\sigma(e_g))$ ^{3}MC one, whereas the donating groups stabilize *both* the ^{3}MLCT and the ^{3}MC level. According to the temperature dependent luminescence behavior, the latter effect (destabilization of ^{3}MC) is more important than the former. For heteroleptic complexes carrying an electron-donating and an electron-accepting substituent, ^{3}MLCT is stabilized much more than for the parent homoleptic complexes (*vide supra*) and ^{3}MC is expected to be stabilized no more than in the $[Ru(tpy\text{-}D)_2]^{2+}$ complexes. As a consequence, the ^{3}MLCT−^{3}MC energy gap is large and luminescence can be observed at room temperature (Table 2).

Low Temperature Radiationless Decay. According to the energy gap law,[44-46] the rate constant of radiationless decay of the ^{3}MLCT excited state to the ground state must *increase* as the energy gap between ground and excited state *decreases*.

(40) Van Houten, J.; Watts, R. J. *Inorg. Chem.* **1978**, *17*, 3381.
(41) Allen, G. H.; White, R. P.; Rillema, D. P.; Meyer, T. J. *J. Am. Chem. Soc.* **1984**, *106*, 2613.
(42) Barigelletti, F.; Juris, A.; Balzani, V.; Belser, P.; von Zelewsky, A. *J. Phys. Chem.* **1987**, *91*, 1095.
(43) A detailed treatment should take into consideration the splitting of the $\pi(t_{2g})$ and $\sigma^*(e_g)$ metal orbitals because the actual symmetry of these complexes is lower than O_h.
(44) Englman, R.; Jortner, J. *J. Mol. Phys.* **1970**, *18*, 145. Freed, F. R.; Jortner, J. *J. Chem. Phys.* **1970**, *52*, 6272.
(45) Freed, F. R. *Acc. Chem. Res.* **1978**, *11*, 74.

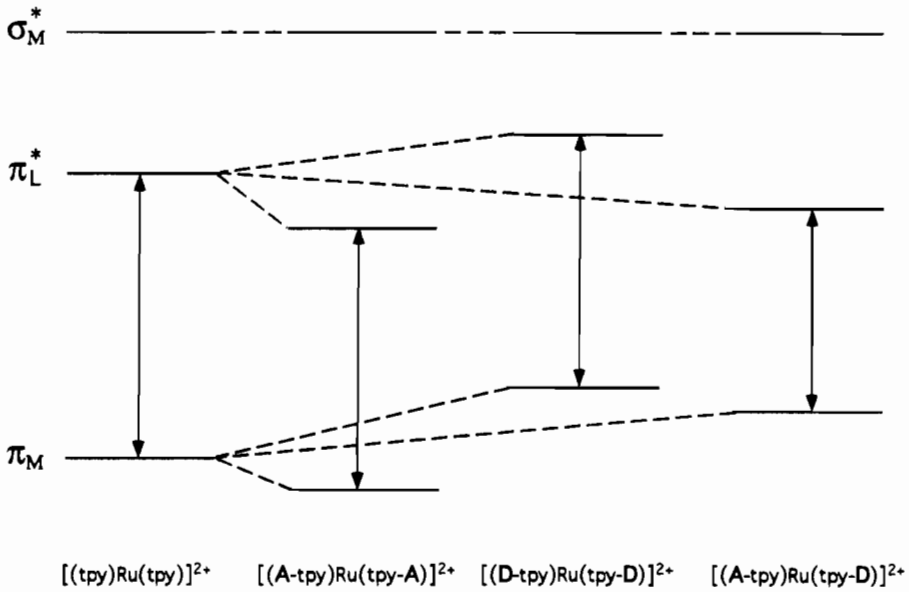

Figure 8. Schematic representation of the effect of electron accepting and electron donating substituents on the energy of the HOMO (π_M) and LUMO (π^*_L) orbitals.

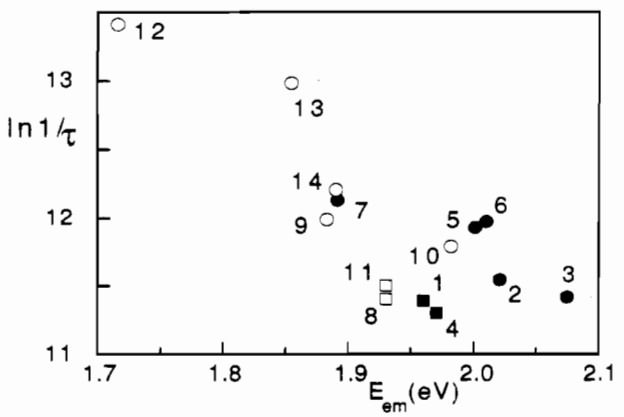

Figure 9. Plot of ln $1/\tau$ (77 K) against the excited state energy. Key: solid symbols, homoleptic complexes; open symbols, heteroleptic complexes.

Because of this effect, complexes with low energy absorption bands typically are weak emitters and have short excited state lifetimes. Figure 9 shows a plot of ln $1/\tau$ (77 K) (that, as we have seen above, is practically equal to the temperature independent radiationless rate constant k_a^{nr}) against the excited state energy. The expected decrease in the rate constant with decreasing excited state energy is observed, but the points are scattered showing that, besides energy gap, specific properties of the complexes play a role. In particular, complexes carrying the $MeSO_2$ and Ph substituents seem to exhibit a smaller radiationless decay rate constant.

The energy gap law, in fact, is based on quantum effects related to the vibrational overlap between the initial and final states in the acceptor modes.[44-46] The rate constant for radiationless decay increases with increasing vibrational overlap. Although the energy gap is usually the most important parameter which affects the overlap, the changes in the equilibrium displacement or frequency between initial (^{3}MLCT) and final (ground) state can also play a role. In its turn, the changes in equilibrium displacement depend on the degree of localization of the π^* antibonding ligand orbital where a nonbonding t_{2g} metal electron is promoted in the ^{3}MLCT excited state. When the π^* orbital is spread over a large molecular framework, more bonds are distorted and the average displacement change is decreased.[47] As far as our compounds are concerned, the electron-withdrawing substituents favour the delocalization of the promoted electron, whereas electron-donor substituents have an opposite effect. This is likely to be the reason why the points in Figure 9 are scattered. The rate constant for $[Ru(tpy\text{-}NMe_2)_2]^{2+}$, in fact, is more than twice that for $[Ru(tpy\text{-}SO_2Me)_2]^{2+}$, in spite of the very similar energy gap. As far as the Ph substituent is concerned, although it is not *per se* an electron-acceptor it can certainly exhibit such a property once tpy has been converted into tpy^-, i.e. in the ^{3}MLCT excited state.

Conclusions

Investigations carried out on 14 $[Ru(tpy\text{-}X)(tpy\text{-}Y)]^{2+}$ complexes (where X and Y are substituents in the 4′ position of 2,2′:6′,2″-terpyridine) have shown that electron-donating (D) or electron-accepting (A) substituents cause dramatic changes in the luminescence and electrochemical properties. Correlations between the Hammett σ parameter and the potentials of the oxidation and reduction processes show that (i) electron-accepting substituents stabilize the LUMO π^* ligand orbital more than the HOMO $\pi(t_{2g})$ metal orbital and (ii) the electron-donor groups destabilize the HOMO $\pi(t_{2g})$ metal orbital more than the LUMO π^* ligand orbital. The latter effect, at first sight unexpected, can be understood by considering that removal of one electron from the metal causes the formation of the electron-accepting Ru^{3+} ion which interacts strongly with the two tpy-D ligands.

As far as the luminescence properties are concerned, two general, and at first sight conflicting, trends have clearly emerged compared with the parent $[Ru(tpy)_2]^{2+}$ complex: (i) the energy of the emission maximum decreases regardless of the electron accepting or electron donating nature of the substituent; (ii) at high temperature, electron-accepting substituents increase the luminescence quantum yield and the excited state lifetime, whereas electron-donating substituents have an opposite effect. These results can be explained on the basis of correlations between the electrochemical potentials and emission

(46) Caspar, J. V.; Westmoreland, T. D.; Allen, G. H.; Bradley, P. G.; Meyer, T. J.; Woodruff, W. H. *J. Am. Chem. Soc.* **1984**, *106*, 349. Kober, E.; Caspar, J. V.; Lumpkin, R. S.; Meyer, T. J. *J. Phys. Chem.* **1986**, *90*, 3722.

(47) Boyde, S.; Strouse, G. F.; Jones, W. E.; Meyer, T. J. *J. Am. Chem. Soc.* **1990**, *112*, 7395.

energies which are made possible by the MLCT nature of the luminescent excited state. It is concluded that when the substituents are electron-accepting groups, the π^* ligand-centered orbital is more stabilized than the $\pi(t_{2g})$ metal-centered orbital because of proximity reasons and the oxidized (in the excited state) metal does not receive any charge compensation from the tpy-A ligand not involved in the electronic transition. When the substituents are electron-donating groups, the π^* ligand-centered orbital is more destabilized than the $\pi(t_{2g})$ metal-centered orbital in the ground state complex, but in the MLCT excited state the $\pi(t_{2g})$ metal orbitals are strongly destabilized because the presence of the tpy-D ligand not involved in the MLCT transition. Heteroleptic complexes carrying an electron-accepting and an electron-donating group always show lower emission energies when compared with the parent homoleptic complexes because the π^* orbital of the tpy-A ligand is stabilized and the tpy-D ligand destabilizes the metal-centered $\pi(t_{2g})$ orbitals. These effects can also explain why the room temperature luminescence quantum yield and lifetime increase on replacing H with electron-accepting substituents and decrease with electron-donating substituents.

Luminescence lifetime measurements at 77 K have shown that the values of rate constants for radiationless decay from ^{3}MLCT to the ground state are governed not only by the energy gap but also by the nature of the substituents which presumably affects the changes in the equilibrium displacement or frequency in going from the excited state to the ground state.

The reported results have shown that it is possible to prepare $Ru(tpy)_2^{2+}$-type complexes which exhibit photophysical properties comparable to those of the $Ru(bpy)_3^{2+}$ family. In view of the synthetic and structural advantages offered by tpy complexes as compared to bpy ones, these results allow the design of new photosensitizers to be used in covalently-linked multicomponent systems for photoinduced energy or electron transfer processes.

Acknowledgments. We would like to thank Professor Franco Scandola for interesting discussions and Miss Paola Taddei for several experimental measurements. This work has been supported by Ministero della Università e della Ricerca Scientifica e Technologica (Italy), Consiglio Nazionale delle Ricerche (Progetto Strategico Tecnologie Chimiche Innovative), the Science and Engineering Research Council (U.K.), and the Schweizerischer Nationalfonds zur Förderung der Wissenschaftlichen Forschung (Switzerland). N.A. thanks NATO for a grant (No. 931569, Supramolecular Chemistry Special Programme).

IC941493+